

Structure-Directing Role of Organoamine Ligands in the Self-Assembly of Novel Bimetallic Oxides[†]

Douglas Hagrman,[‡] Christopher J. Warren,[§]
Robert C. Haushalter,[§] Candace Seip,[‡]
Charles J. O'Connor,[‡] Randy S. Rarig, Jr.,^{||}
Kenneth M. Johnson, III,^{||}
Robert L. LaDuca, Jr.,^{||} and Jon Zubieta^{*‡}

Department of Chemistry, Syracuse University,
111 College Place, Syracuse, New York 13244-4100,
Symyx Technologies, 3100 Central Expressway,
Santa Clara, California 95051, King's College,
Briarcliff, New York, and University of New Orleans,
New Orleans, Louisiana

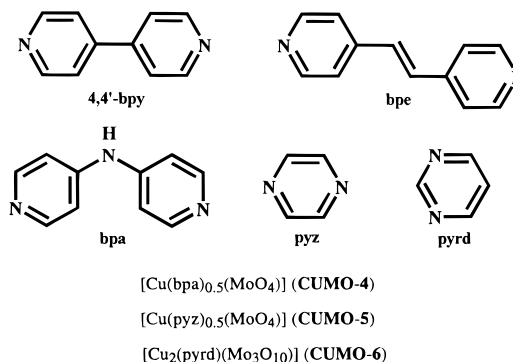
Received June 22, 1998

Revised Manuscript Received August 21, 1998

Solid-state oxides exist for the majority of the elements, making these materials ubiquitous in the geosphere and in the biosphere.^{1,2} While many naturally occurring oxides and minerals possess complex crystal structures, the majority are of simple composition and have highly symmetrical structures and rather small unit cells. Although such simple oxides may possess unique properties, such as piezoelectricity, ferromagnetism, or catalytic or sorptive activity, as a general rule there is a correlation between the complexity of the structure of a material and its functionality.³ In the realm of biomineralization,⁴ for example, the inorganic oxide contributes to the increased functionality via incorporation as one component in a hierarchical structure where there is a synergistic interaction between an organic and inorganic component.^{5,6} Since the interaction within these hybrid organic–inorganic materials derives from the nature of the interface between the organic component and the inorganic oxide, synthetic and structural studies of materials exhibiting such an interface should allow an evolution of the understanding of strategies for controlling structure–property relationships for these hybrid materials.

Four major classes of oxides in which organic materials play an important structural role have been identified: zeolites,⁷ mesoporous oxides,⁸ biomineralized materials, and microporous octahedral–tetrahedral frame-

work transition metal phosphates with entrained organic cations.⁹ A potential fifth class was recently described by us: hybrid solids constructed from one-dimensional coordination of polymer matrixes and molybdenum oxide subunits.¹⁰ By exploiting the structure-directing role of polyfunctional rodlike organoamine ligands,¹¹ the bimetallic oxides [$\{\text{Cu}(4, 4'\text{-bpy})\}_4\text{Mo}_8\text{O}_{26}\}$ (**CUMO-1**) and [$\{\text{Cu}(4, 4'\text{-bpy})\}_4\text{Mo}_{15}\text{O}_{47}\}$ (**CUMO-2**) were isolated and shown to contain $\{\text{Cu}(4, 4'\text{-bpy})\}^{+1}$ -linked polyoxomolybdate clusters and one-dimensional molybdenum oxide chains, respectively.¹² More recently, we demonstrated that small geometric perturbations of the ligand can produce dramatic changes in the oxide geometry with the characterization of $[\text{Cu}(\text{bpe})(\text{MoO}_4)]$ (**CUMO-3**, bpe = 1,2-bis(4-pyridyl)ethene), a material with a three-dimensional covalent framework and a two-dimensional $\{\text{Cu}(\text{MoO}_4)\}$ metal oxide network.¹³ To assess the role of ligand geometry in directing the self-assembly of copper–molybdenum oxides, the relative geometry of the donor groups was modified by introducing a linker which constrains the donors into a different relative orientation, as in bipyridylamine (bpa), and by decreasing the donor-to-donor distance in pyrazine (pyz) and pyrimidine (pyrd). The profound influence of the organic component on the structure of such hybrid materials was realized in the preparation of three novel copper molybdates with entrained organoamine ligands, $[\text{Cu}(\text{bpa})_{0.5}(\text{MoO}_4)]$ (**CUMO-4**), $[\text{Cu}(\text{pyz})_{0.5}(\text{MoO}_4)]$ (**CUMO-5**), and $[\text{Cu}_2(\text{pyrd})(\text{Mo}_3\text{O}_{10})]$ (**CUMO-6**).



To preserve the structural elements of the organic component, the syntheses of these solid-state materials

[†] Dedicated to Professor Achim Müller on the occasion of his 60th birthday.

[‡] Syracuse University.

[§] Symyx Technologies.

[‡] University of New Orleans

^{||} King's College.

(1) Wells, A. F. *Structural Inorganic Chemistry*, 4th ed.; Oxford University Press: Oxford, 1975.

(2) Greenwood, N. N.; Earnshaw, A. *Chemistry of the Elements*; Pergamon Press: New York, 1984.

(3) Stupp, S. I.; Braun, P. V. *Science* **1997**, *277*, 1242.

(4) Hench, L. L. In *Materials Chemistry An Emerging Discipline*; Interrante, L. V., Caspar, L. A., Ellis, A. B.; ACS Symp. Ser. 245; American Chemical Society: Washington, DC, 1995; Chapter 21, p 523.

(5) Mann, S. *Nature* **1993**, *365*, 499.

(6) Zaremba, C. M.; Belcher, A. M.; Fritz, M.; Li, Y.; Mann, S.; Hansma, P. K.; Morse, D. E.; Speck, J. S.; Stucky, G. D. *Chem. Mater.* **1996**, *8*, 678.

(7) (a) Smith, J. V. *Chem. Rev.* **1988**, *88*, 149. (b) Occelli, M. L.; Robson, H. C. *Zeolite Syntheses*; American Chemical Society: Washington, DC, 1989.

(8) Kresge, C. T.; Leonowicz, M. E.; Roth, W. J.; Vartuli, J. C.; Beck, J. S. *Nature*, **1992**, *359*, 710.

(9) (a) Haushalter, R. C.; Mundi, L. A. *Chem. Mater.* **1992**, *4*, 31. (b) Khan, M. I.; Myer, L. M.; Haushalter, R. C.; Schweitzer, A. L.; Zubieta, J.; Dye, J. L. *Chem. Mater.* **1996**, *8*, 43.

(10) Hagrman, D.; Zubieta, C.; Rose, D. J.; Zubieta, J.; Haushalter, R. C. *Angew. Chem., Int. Ed. Engl.* **1997**, *36*, 873.

(11) See, for example: Robinson, F.; Zaworotko, M. J. *J. Chem. Soc., Chem. Commun.* **1995**, 2413; Yaghi, O. M.; Li, H. *J. Am. Chem. Soc.* **1996**, *118*, 295; Batsanov, A. S.; Begley, M. J.; Hubberstey, P.; Stroud, J. *J. Chem. Soc., Dalton Trans.* **1996**, 1947; Blake, A. J.; Champness, N. R.; Khlobystov, A. N.; Lemenovskii, D. A.; Li, W.-S.; Schroder, M. *Chem. Commun.* **1997**, 1339; Blake, A. J.; Champness, N. R.; Khlobystov, A.; Lemenovskii, D. A.; Li, W.-S.; Schroder, M. *Chem. Commun.* **1997**, 2027.

(12) We have also shown that 2, 2'-bipyridine is effective in the self-assembly of copper molybdates such as $[\text{Cu}(2,2'\text{-bpy})\text{Mo}_2\text{O}_7]$ (**CUMO-7**): Zapf, P. J.; Warren, C. J.; Haushalter, R. C.; Zubieta, J. *Chem. Commun.* **1997**, 1543.

(13) Hagrman, D.; Haushalter, R. C.; Zubieta, J. *Chem. Mater.* **1998**, *10*, 0, in press.

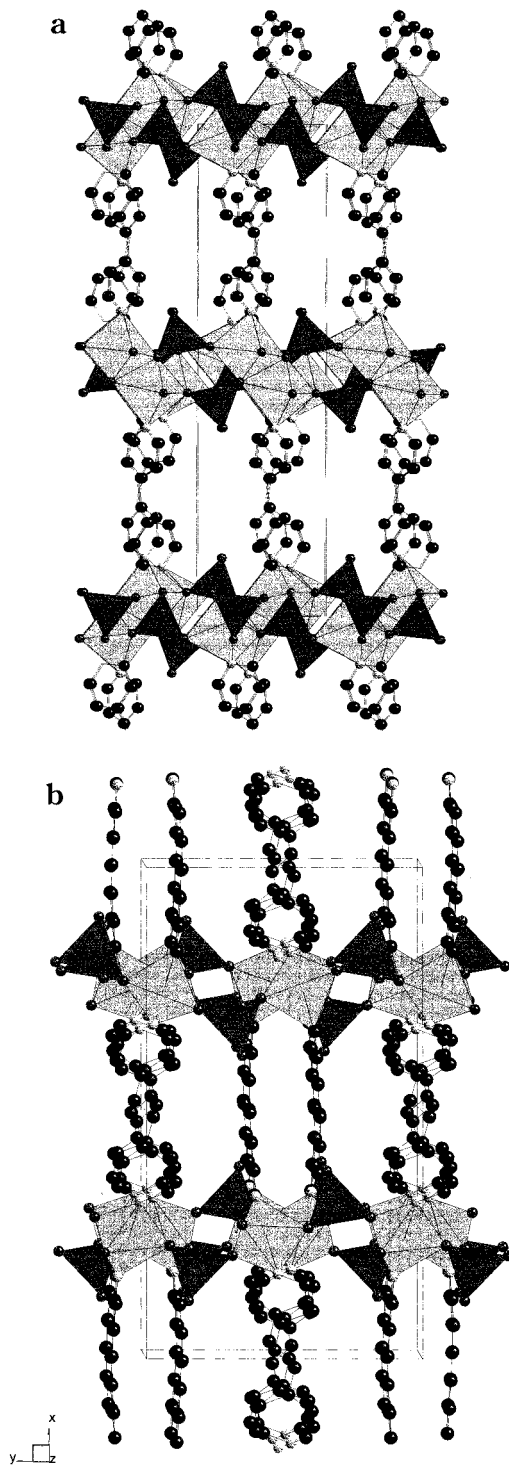


Figure 1. (a) A view of the structure of **CUMO-4**, along the c axis, illustrating the three-dimensional framework constructed from $\{\text{CuMoO}_4\}$ oxide layers linked through bpa bridges. This is the characteristic alternating organic-inorganic layer pattern associated with such composite solids. (b) A view of the unit cell packing of $[\text{Cu}(\text{bpe})\text{MoO}_4]$ (**CUMO-3**), viewed down the c axis. The bend introduced by the ethylene bridge of the bpe ligand is evident in the ligand groups viewed face-on at the edges of the cell.

exploited hydrothermal techniques, conditions which also favor the isolation of metastable phases and which encourage crystal growth from solution.¹⁴ In a repre-

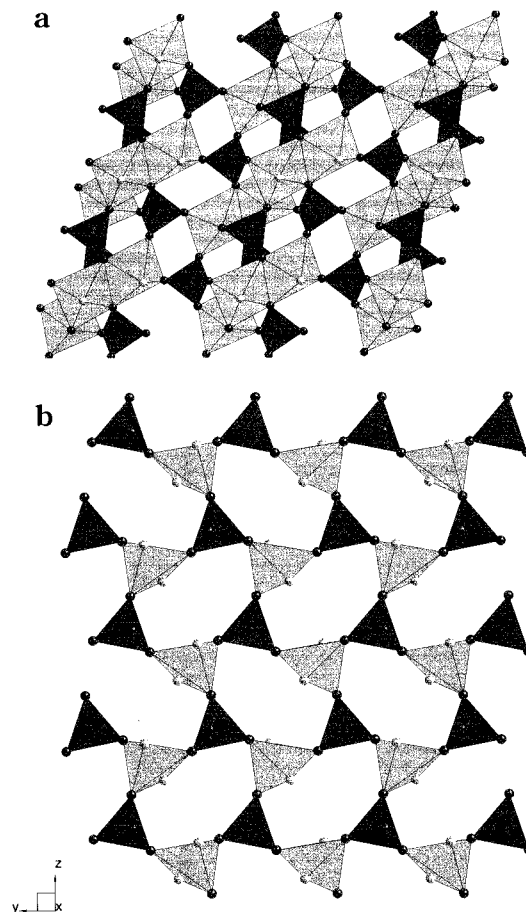


Figure 2. (a) A view down the b -axis of the unique $\{\text{CuMoO}_4\}$ layer structure of **CUMO-4**. (b) A view down the a -axis of the layer structure of **CUMO-3**.

sentative synthesis, a mixture of MoO_3 , $\text{Cu}(\text{NO}_3)_2 \cdot 2.5\text{H}_2\text{O}$, pyrazine, and H_2O in the mole ratio 1:1.1:1.4:1927 was heated at 180°C for 78 h to give dark green crystals of $[\text{Cu}(\text{pyz})_{0.5}(\text{MoO}_4)]$ (**CUMO-5**) in 30% yield.¹⁵

As shown in Figure 1a, the structure of $[\text{Cu}(\text{bpa})_{0.5}\text{MoO}_4]$ (**CUMO-4**)¹⁶ consists of $\{\text{CuMoO}_4\}$ bimetallic oxide layers covalently linked through bpa ligands into a three-dimensional framework. The structure exhibits the pattern of alternating organic-inorganic regions characteristic of the metal-organophosphate phases.¹⁷

(15) The methods for syntheses are as follows. $[\text{Cu}(\text{bpa})_{0.5}\text{MoO}_4]$: A mixture of MoO_3 (0.043 g), $\text{Cu}(\text{NO}_3)_2 \cdot 2.5\text{H}_2\text{O}$ (0.056 g), 4,4'-dipyridylamine (0.072 g), and H_2O (10 mL) in the mole ratio 1.2:1.1:1.7:2190 was heated at 180°C for 66.5 h in a Parr acid digestion bomb. Light green crystals of **CUMO-4** were collected in 60% yield (based on Cu). IR (KBr pellet, cm^{-1}): 3438 (s), 1640 (m), 1614 (s), 1429 (w), 1387 (m), 948 (m), 880 (m), 821 (s), 788 (s), 737 (s), 669 (m). $[\text{Cu}(\text{pyz})_{0.5}\text{MoO}_4]$: A mixture of MoO_3 (0.043 g), $\text{Cu}(\text{NO}_3)_2 \cdot 2.5\text{H}_2\text{O}$ (0.076 g), pyrazine (0.033 g) and H_2O (10 mL) in the mole ratio 1:1.1:1.4:1927 was heated at 180°C for 78 h in a Parr acid digestion bomb. Dark green crystals of **CUMO-5** were recovered in 30% yield. IR (KBr pellet, cm^{-1}): 1633 (m), 1415 (s), 1886 (m), 1122 (m), 1070 (m), 918 (s), 797 (vs, br), 478 (s). $[\text{Cu}_2(\text{pyrd})\text{Mo}_3\text{O}_{10}]$: A mixture of MoO_3 (0.044 g), $\text{Cu}(\text{NO}_3)_2 \cdot 2.5\text{H}_2\text{O}$ (0.077 g), pyrimidine (0.031 g), and H_2O (10 mL) in the mole ratio 1:1:1.25:1823 was heated at 160°C for 72 h to give dark purple-black crystals of **CUMO-6** in 95% yield (based on Mo). IR (KBr pellet, cm^{-1}): 2353 (m), 1594 (m), 1381 (w) 866 (vs), 706 (m), 660 (s), 544 (s).

(16) **CUMO-4**, $\text{C}_{10}\text{H}_9\text{Cu}_2\text{Mo}_2\text{N}_3\text{O}_{11}$: monoclinic, $P2_1/c$, $a = 7.5233$ (4) Å, $b = 27.4599$ (14) Å, $c = 9.2537$ (5) Å, $\beta = 108.27$ (1)°, $V = 1815.3$ (2) Å³, $Z = 4$, $D_{\text{calc}} = 2.437\text{ g cm}^{-3}$; structure solution and refinement based on 4229 reflections converged at $R1 = 0.0681$, $wR2 = 0.1172$. Further details on the crystal structure investigations may be obtained on application to The Director, CCDC, 12 Union Road, Cambridge CB21EZ, UK and citing the supplementary publication no. CCDC-101607.

(14) Gopalakrishnan, J. *Chem. Mater.* **1995**, *7*, 1265.

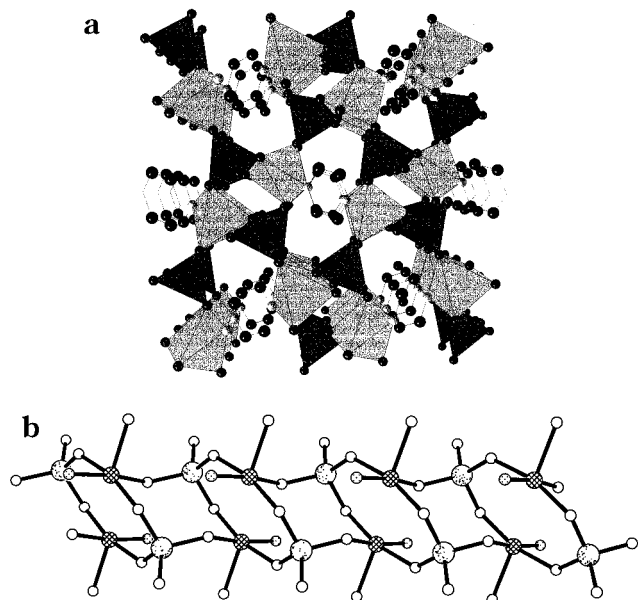


Figure 3. (a) A view of the structure of **CUMO-5**, along the axis, highlighting the channels occupied by the pyrazine bridges. (b) One $\{\text{CuMoO}_4\}$ chain of **CUMO-5**.

The inorganic layer, shown in Figure 2a, is constructed from $\{\text{MoO}_4\}$ tetrahedra and $\{\text{CuO}_5\text{N}\}$ octahedra which form double chains linked through $\{\text{Cu}-\text{O}-\text{Mo}\}$ bridges into a two-dimensional network. One Cu site forms corner-sharing interactions with the five adjacent Mo sites of the chain, while the second Cu site forms four corner-sharing linkages to Mo chain sites and one to an Mo site of an adjacent chain. In addition, the two unique Cu sites form a binuclear edge-sharing unit through a $\{\text{Cu}_2\text{O}_2\}$ interaction. One Mo site bridges three Cu binuclear units of a given chain and provides linkage to an adjacent chain through its fourth oxo group. The second Mo site bridges three Cu binuclear units of the chain and projects a terminal oxo group into the interlamellar region.

In comparing **CUMO-4** to $[\text{Cu}(\text{bpe})\text{MoO}_4]$ (**CUMO-3**), the influence of ligand types on oxide structure is revealed. In contrast to **CUMO-3**, which contains $\{\text{Cu}-\text{bpe}-\text{Cu}-\}$ chains with $\{\text{CuO}_4\text{N}_2\}$ coordination geometry, **CUMO-4** exhibits $\{\text{Cu}-\text{bpa}-\text{Cu}-\}$ binuclear units, that is, there is no $\{\text{Cu}-\text{diamine}-\text{Cu}-\}$ chain propagation and the coordination geometry is $\{\text{CuO}_5\text{N}\}$. As shown in Figure 2b, the layer structure adopted by **CUMO-3** consists of simple $\{\text{Cu}_3\text{Mo}_3\text{O}_6\}$ fused rings rather than the more complex connectivity enjoyed by **CUMO-4**. The consequences of ligand geometry are also manifest in the packing diagrams for **CUMO-3** and **CUMO-4**, shown in parts a and b of Figure 1, respectively.

Two contrasting geometric features of the ligands bpa and bpe are evident: the angles between the donor groups and the Cu-Cu distances imposed by linker length, 11.74 Å vs 13.56 Å for **CUMO-4** and **CUMO-3**, respectively. To assess the influence of donor group separation on structure, the oxide $[\text{Cu}(\text{pyz})_{0.5}\text{MoO}_4]$ (**CUMO-5**) was prepared. As shown in Figure 3, the structure¹⁸ consists of a complex three-dimensional bimetallic oxide with channels occupied by the pyrazine ligand. The structure is constructed from corner-

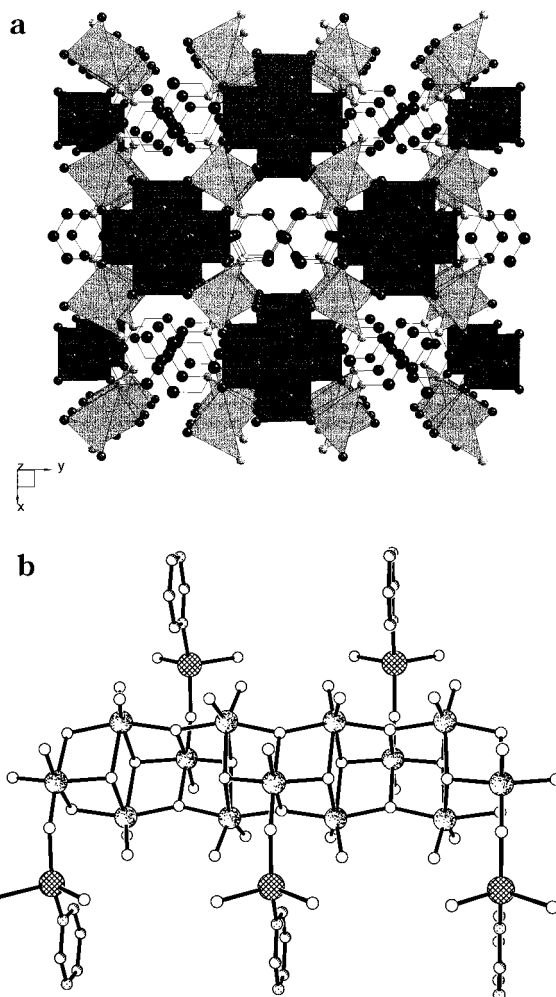


Figure 4. (a) A view of the three-dimensional structure of **CUMO-6**, highlighting the channel occupied by the pyrimidine bridges. (b) A view of the $\{\text{Mo}_3\text{O}_{10}\}^{n-}$ chains and the appended $\{\text{Cu}(\text{pyrd})\}$ groups which serve to bridge adjacent chains.

sharing $\{\text{MoO}_4\}$ tetrahedra and $\{\text{CuO}_4\text{N}\}$ square pyramids, which form chains of stacked $\{\text{Cu}_2\text{Mo}_2\text{O}_4\}$ rings. Each Mo site links three adjacent Cu sites of a chain and employs the fourth oxo group to connect to an adjacent chain. Four adjacent chains are linked to form a cavity occupied by the pyrazines which serve to ligate to Cu sites of opposite chains.

An obvious geometric variant is provided by pyrimidine, which was exploited in the synthesis of $[\text{Cu}_2(\text{pyrd})\text{Mo}_3\text{O}_{10}]$ (**CUMO-6**), a structure¹⁹ constructed from $\{\text{MoO}_6\}$ octahedra and $\{\text{CuO}_3\text{N}\}$ tetrahedra, which link to form a three-dimensional bimetallic oxide framework with channels occupied by the pyrimidine groups. As shown in Figure 4, the $\{\text{MoO}_6\}$ octahedra form a chain of edge-sharing polyhedra, structurally analogous to that observed for the one-dimensional $(\text{NH}_4)_2[\text{Mo}_3\text{O}_{10}]$.²⁰ Each Cu site coordinates to two oxo groups of two Mo

(18) **CUMO-5**, $\text{C}_4\text{H}_4\text{Cu}_2\text{Mo}_2\text{N}_2\text{O}_8$; monoclinic $P2_1/n$, $a = 5.1894(4)$ Å, $b = 11.9100(7)$ Å, $c = 8.2030(5)$ Å, $\beta = 102.413(2)^\circ$, $V = 495.14(6)$ Å³, $Z = 2$, $D_{\text{calc}} = 3.535$ g cm⁻³; structure solution and refinement based on 1007 reflections converged at $R1 = 0.0338$ and $wR2 = 0.0816$ (CCDC-101608).

(19) **CUMO-6**, $\text{C}_4\text{H}_4\text{Cu}_2\text{Mo}_3\text{N}_2\text{O}_{10}$; orthorhombic $Cmcm$, $a = 12.4422(2)$ Å, $b = 12.1223(3)$ Å, $c = 7.6790(2)$ Å, $V = 1158.21(5)$ Å³, $Z = 4$, $D_{\text{calc}} = 3.756$ g cm⁻³; structure solution and refinement based on 791 reflections converged at $R1 = 0.0334$ and $wR2 = 0.0771$ (CCDC-101609).

(17) Khan, M. I.; Zubieta, J. *Prog. Inorg. Chem.* **1995**, *43*, 1.

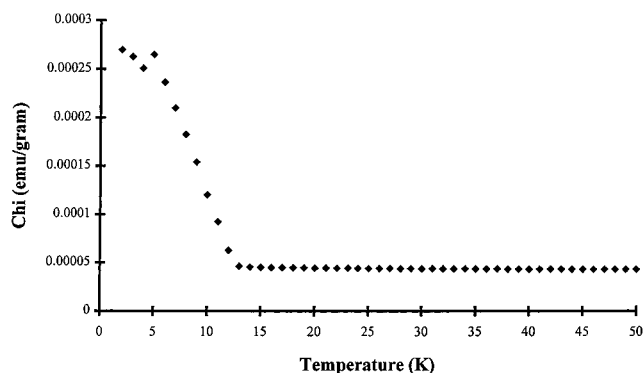


Figure 5. Magnetic susceptibility of **CUMO-6** plotted as a function of temperature after cooling in a magnetic field of 50 G. The measuring field is also 50 G.

sites of one chain and bridges an adjacent chain by bonding to one oxo group. In addition, each Cu center coordinates to a nitrogen donor of a pyrimidine ligand, which serves to bridge to a second Cu site through its second nitrogen donor. When viewed along the crystallographic *a* axis, the Mo oxide chains are linked through stacked $\{\text{CuO}_3\text{N}\}$ tetrahedra to produce channels of sufficient diameter to accommodate parallel interdigitated stacks of pyrimidine groups.

It is noteworthy that crystals of **CUMO-6** are black, indicative of a mixed valence state. Valence sum calculations²¹ provide an average oxidation state of +5.7 for the Mo sites; curiously, the Cu sites exhibit an average oxidation state of +1.5, suggesting extensive electronic delocalization. The resulting magnetic susceptibility behavior²² shown in Figure 5 is unusual. **CUMO-6** exhibits a room temperature magnetic moment of $0.113\mu_{\text{B}}$. The temperature dependent magnetic susceptibility data show a magnetic transition at 13 K. From the appearance of the susceptibility, this is most likely a transition to a ferrimagnetic or canted antiferromagnetic state. However, no satisfactory fit to a model could be derived. Below the transition temperature, the sample exhibits hysteresis with a remanent magnetization, M_r , of 0.017 emu g^{-1} and coercivity, H_c , of 750 G.

The thermal decompositions of **CUMO-4** and **CUMO-5** under nitrogen atmosphere exhibit release of

ligand in the 350–450 °C range to yield $[\text{CuMoO}_4]$ and a mixture of $[\text{CuMoO}_4]$ and $[\text{MoO}_2]$, respectively. In contrast, **CUMO-6** exhibits a weight loss of ca. 25% in the 375–450 °C range in two steps, corresponding to the loss of ligand and reduction to give a black material analyzing as $[\text{Cu}_2\text{Mo}_3\text{O}_6]$ with a powder diffraction profile distinct from those of known copper molybdates or simple molybdenum oxides. This observation suggests that thermal treatment of such organic–inorganic composite materials may provide a route to new bimetallic oxides. We are investigating the properties of such products of thermal decomposition for the **CUMO** class and related families of mixed metal oxides templated by organoamine ligands.

The isolation and characterization of the materials of this study illustrate the dramatic structural influence of organic components on the microstructure of inorganic oxides. While the structure-directing function of the organic group is in the broadest perspective related to factors such as donor-group orientation, space-filling and steric constraints, and differential solubilities, the specific role of ligand geometry, in the sense of relative donor-group dispositions and organic tether length, is revealed in the structures of this study. Thus, the contrasting structures of **CUMO-3** and **CUMO-4** derive from the angular perturbation and spatial extension at the ligand tether. Similarly, the structures of **CUMO-5** and **CUMO-6** are unique expressions of the folding of the oxide substructure about the spatially restricted diamine ligands to generate channel structures. The different oxide frameworks of **CUMO-5** and **CUMO-6** reflect the requirements imposed by the donor-group dispositions in pyrazine and pyrimidine, respectively. It is noteworthy that the general strategy of employing organic components to modify inorganic substructures has witnessed a parallel development in the elaboration of the metal halides.²⁴

Acknowledgment. This work was supported by NSF grant CHE9617232

Supporting Information Available: X-ray crystal data for **CUMO-4–6** (16 pages). Ordering information is given on any current masthead page.

CM980439E

(20) (a) Range, K.; Fässler, A. *Acta Crystallogr., Sect. C* **1990**, *46*, 488. (b) Xu, Y.; An, L.-H.; Koh, L.-L. *Chem. Mater.* **1996**, *8*, 814.

(21) Brown, I. D.; Wu, K. K. *Acta Crystallogr., Sect. B*, **1976**, *32*, 1957.

(22) The magnetic susceptibility data were recorded on a 23.22 mg polycrystalline sample of $[\text{Cu}_2(\text{pyridazine})\text{Mo}_3\text{O}_{10}]$ over a temperature range of 2–300 K using a Quantum Design MPMS-5S SQUID susceptometer. Measurement and calibration techniques have been reported elsewhere.²¹ The temperature-dependent magnetic data were measured at magnetic fields of 1000 and 50 G. Magnetism was also recorded as the magnetic field was cycled between 50 000 and –50 000 G at a temperature of 2 K.

(23) O'Connor, C. J. *Prog. Inorg. Chem.* **1982**, *29*, 203.

(24) See, for example: (a) Wang, S.; Mitzi, D. B.; Landrum, G. A.; Genin, H.; Hoffmann, R. *J. Am. Chem. Soc.* **1997**, *119*, 724 and references therein; (b) DeBord, J. R. D.; Lu, Y.-J.; Warren, C. J.; Haushalter, R. C.; Zubieta, J. *Chem. Commun.* **1997**, 1368. (c) Chakravarty, V.; Guloy, A. M. *Chem. Commun.* **1997**, 697. (d) Corradi, A. B.; Cramarossa, M. R.; Saladini, M. *Inorg. Chim. Acta* **1997**, *257*, 19. (e) Masciocchi, N.; Cairati, P.; Carlucci, L.; Mezza, G.; Ciani, G.; Sironi, A. *J. Chem. Soc., Dalton Trans* **1996**, 2739. (f) Mitzi, D. B. *Chem. Mater.* **1996**, *8*, 791. (g) Ayllón, J. A.; Santos, J. C.; Henriques, R. T.; Almeida, M.; Alcácer, L.; Duarte, M. T. *Inorg. Chem.* **1996**, *35*, 168.